Meas. Sci. Technol. **11** (2000) 712–716. Printed in the UK PII: S0957-0233(00)12036-3

Laser-based distance measurement using picosecond resolution time-correlated single-photon counting

Sara Pellegrini†‖, Gerald S Buller†, Jason M Smith†, Andrew M Wallace‡ and Sergio Cova§

† Department of Physics, Heriot-Watt University, Riccarton, Edinburgh EH14 4AS, UK
‡ Department of Computing and Electrical Engineering, Heriot-Watt University, Riccarton, Edinburgh EH14 4AS, UK
§ Dipartimento di Elettronica e Informazione, Politecnico di Milano, Milano, Italy

E-mail: S.Pellegrini@hw.ac.uk

Received 22 February 2000, in final form 14 March 2000, accepted for publication 22 March 2000

Abstract. In this paper, we report results obtained with a time-of-flight ranging/scanning system based on time-correlated single-photon counting. This system uses a pulsed picosecond diode laser and detects the scattered signal from a non-cooperative target surface using a semiconductor single-photon detector. A demonstration system has been constructed and used to examine the depth resolution obtainable as a function of the integrated number of photon returns. The depth resolution has been examined for integrated photon returns varying by five orders of magnitude, both by obtaining experimental measurements and by computer simulation. Depth resolutions of approximately 3 mm were obtained for only ten returned photons. The effect of the background signal, originating either from temporally uncorrelated light signals or from detector noise, has also been examined.

Keywords: distance, time-correlated single-photon counting, pulsed picosecond laser, single-photon avalanche diode, machine vision, ranging

1. Introduction

In the last few years, depth profiling using a time-of-flight (TOF) system utilizing time-correlated single-photon counting (TCSPC) has successfully been demonstrated [1–3]. Using this approach, laser pulses of duration $\simeq$ 15 ps are directed towards a non-cooperative target and a single-photon detector is used to detect the scattered signal. To reduce the effect of drift in the timing system, an additional reference target was used and the distance to the target was proportional to the time delay between the scattered and reference signals. Previous work [1, 2] used the TOF system for very accurate scanning of surfaces at very short range (i.e. approximately 20 μm depth resolution at 2 m). In this paper we will discuss recent studies on the use of this technique for distance measurements using low numbers of integrated photon returns (i.e. $N \geqslant 10$), which is consistent with short acquisition times, long distance measurements, poorly scattering objects and oblique surfaces. Experimental results are presented and compared with simulations, to give an estimate of the resolution attainable under these conditions.

‖ On exchange from the Politecnico di Milano, Piazza Leonardo da Vinci 32, Milano 20133, Italy.

2. The system hardware and experimental measurements

Figure 1 is a schematic diagram of the depth profiling system. The laser source used was a passively Q-switched AlGaAs/GaAs laser diode [4] emitting 10 ps duration pulses with 10 pJ energy per pulse, at a wavelength of $\simeq$ 850 nm. A pulse repetition rate of about 25 MHz was used in this work. In this work, a silicon-based single-photon avalanche diode (SPAD) detector [5] was used. When the SPAD is reverse biased above the breakdown voltage, a single photon absorbed in the depletion region can initiate an avalanche process, which produces a detectable current (up to a few milli-amperes). Besides the general advantages found in using solid-state devices, compared with photomultipliers, SPAD detectors exhibit superior photon detection efficiency and faster and cleaner time responses [6, 7]. The instrumental jitter for evaluation of the laser pulse arrival time can be less than 50 ps. The small active area ($\simeq$20 μm diameter)

0957-0233/00/060712+05$30.00

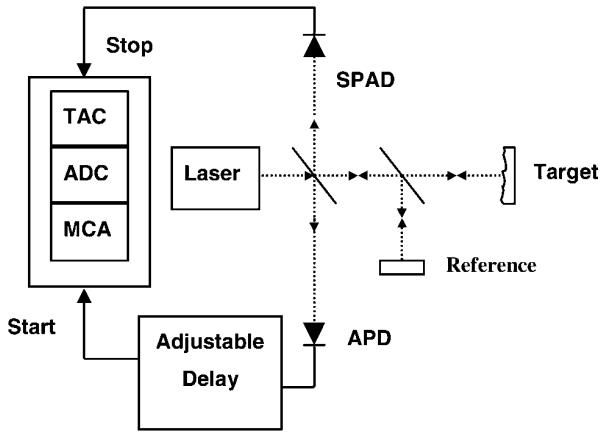

Figure 1. A schematic diagram of a TCSPC ranging system, indicating the main components. The avalanche photodiode (APD) provides an analogue electrical signal to start the timing process of the time-to-amplitude converter (TAC). The TAC output is digitized using an analogue-to-digital converter (ADC) and stored in the multichannel analyser (MCA). In the experiments described, the reference arm used was an optical fibre whose length was chosen in order to position the reference signal close to the expected target return.

presents a considerable advantage in these applications, making possible high spatial resolution and low sensitivity to spurious backscattering. An active quenching circuit (AQC) is used to fully exploit the performance of the detector [5]. The AQC senses the avalanche process in the SPAD, provides a digital output pulse synchronous with the arrival time of the photon, then quenches the avalanche and, after a predetermined time, reapplies the reverse bias to the SPAD, thus leaving it ready to receive the next photon.

The timing process is performed by a time-to-amplitude converter (TAC). The TAC is started by a signal from the analogue avalanche photodiode (APD, Hamamatsu C5658), which detects a signal directly from the laser pulse. The TAC is stopped on the detection of a photon event via the AQC. The TAC output is an analogue signal proportional to the time elapsed between the start and stop signals. It is digitized using an analogue-to-digital converter (ADC) and stored in a multi-channel analyser (MCA). In the experiments reported in this paper, the TAC, ADC and MCA are integrated onto a single plug-in card (Becker & Hickle SPC-300) for an IBM-compatible personal computer. This system has a maximum data acquisition rate of approximately 2 MHz. Both the target and the reference signals are detected by the same SPAD. In the experiments shown, the reference is optically delayed by a length of optical fibre in order to temporally position the reference signal close to the target return, thus permitting the use of the highest time resolution window. In the experiments reported here the MCA histogram bin width is typically only 2.44 ps; hence, with only 4096 channels (i.e. $\simeq$10 ns MCA window) used, it is vital that the reference can be independently positioned close to, but not overlapping, the target signal. In addition, an electrical delay is used to position both reference and target peaks within the MCA window.

When the laser pulses are repeated many times, the MCA builds up a histogram of the photon arrival times, thus obtaining an accurate representation of the probability

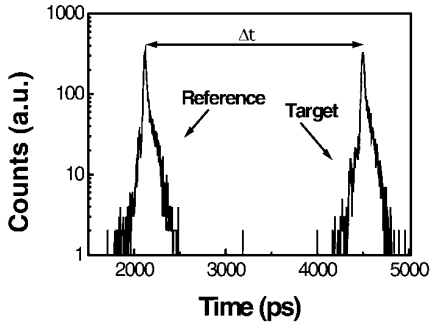

Figure 2. A histogram of raw data for an integrated number of counts $N = 5 \times 10^5$. The peak on the left-hand side is formed by the counts added to each channel by the detection of photons reflected from the reference surface, while the one on the right-hand side is made up from the photons scattered from the target surface.

distribution of arrival times of returning photons. Figure 2 shows an example of the type of histogram produced in a typical ranging measurement, the two peaks corresponding to the known reference surface and to the (non-cooperative) target. In this case the delay between the target and the reference is about $\Delta t = 2.38$ ns and the distance of the target can be calculated using the following formula:

$$Z_{target} = Z_{reference} + \frac{c \times \Delta t}{2}$$

where $Z_{reference}$ is the position of the reference peak, calculated as

$$Z_{reference} = l_{of} n_{of}$$

where l_{of} is the length of the optical fibre and n_{of} is its effective refractive index. Since $Z_{reference} = 2.59$ m, the distance of the target is $Z_{target} = 2.947$ m.

The background noise with this set-up is very small, which is shown by the low number of counts in the region between the two optical signals. The origin of the counts seen between the optical pulses is either ambient light (which is not correlated to the laser pulse) or the phenomenon of 'dark counts', which are mainly caused by thermally generated carriers initiating the avalanche process.

In these experiments, the target was placed approximately 3 m from the optical head. The target used was a light-coloured piece of cardboard, which had no significant specular reflection. The distance of 3 m was chosen since it was the longest achievable in the laboratory for this feasibility study. In order to achieve a small number of returned photons, the acquisition time was set to the minimum time allowable on the Becker and Hickle card, which was 10 ms. At this acquisition time the maximum number of total integrated counts was $N = 10$. For additional attenuation, neutral density filters were used to attenuate both the incident laser and the scattered return signal. It should be noted that later generations of these cards allow even shorter acquisition times [8] of 100 μs, thus permitting the possibility of rapid xyz data point acquisition when they are operated in conjunction with a scanning head. Another advantage of a short acquisition time, besides a potential for very fast surface scanning, is a corresponding reduction in the uncorrelated counts associated with the background due to ambient light or 'dark' counts

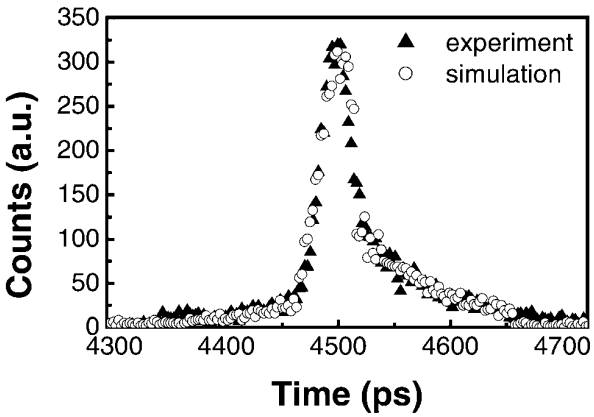

Figure 3. A comparison between the simulated and the experimental histograms representing the scattered return from the target for $N = 10^4$.

of the detector, provided that the intensity of this background is low with respect to that of the scattered signal.

3. The simulation of experimental results

To test the behaviour of our system for a very small number of counts, we simulated the raw data by generating a histogram with similar characteristics to the experimental results. The model resembles the MCA behaviour in terms of the storage of data in the different channels. Each time a photon is detected, the MCA adds one count to the channel that corresponds to the arrival time of the detected photon. In the simulation one count is added to a channel of the histogram according to a probability distribution that resembles the pulse generated by the instrumental response (figure 3). According to the histogram corresponding to the measurements, it was found that the function that fits best the instrumental response had a central peak shape which was Gaussian and an exponential rise and fall on either side of the Gaussian (with different time constants in each case). The simulated curve has the following equation:

$$f(t) = \begin{cases} C_1 \exp[(t - t_1)/\tau_1] & t < t_1 \\ \exp[-(t - t_0)^2/(2\sigma^2)] & t_1 \leqslant t \leqslant t_2 \\ C_2 \exp[(t - t_2)/\tau_2] & t_2 < t \leqslant t_3 \\ C_3 \exp[(t - t_3)/\tau_3] & t > t_3 \end{cases} \quad (1)$$

where C_1, C_2 and C_3 are multiplicative constants and t_0 is the time position of the peak maximum. t_1, t_2 and t_3 are the points at which the changeovers between the central Gaussian and the three exponential functions occur. These parameters were selected on the basis of accurate experimental measurements based on a large integrated photon return, i.e. $N > 10^6$. The algorithm we used to simulate the raw data calculates the arrival time of each photon. These times were distributed to the appropriate channel according to the probability determined by equation (1). The width of the curve is due to several effects, namely the laser pulse width, the response jitter of the detection system, the size of the laser spot and other minor effects.

To determine the accuracy of the system experimentally, 20 sets of measurements were taken, all having the same

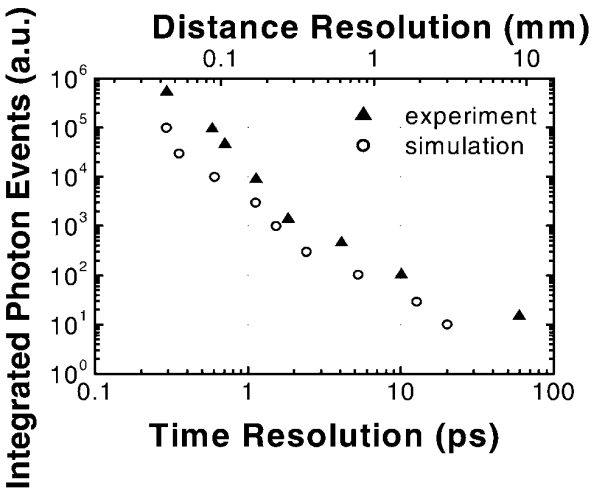

Figure 4. The integrated number of photon events versus distance and time resolutions. Both the experimental results and the theoretical ones are plotted. The data follow a straight line, corresponding to equation (2).

distance between the reference and the target and the same number of counts N, subject to fluctuations governed by Poissonian statistics. This was repeated seven times for different values of N in the range 10 to 10^6. This large variation in N was achieved experimentally by using a constant acquisition time of 10 ms and appropriately attenuating the return signal for the data sets of $N = 10$, 10^2, 10^3 and 10^4. Increases in acquisition time to 100 ms for $N = 10^5$ and 1000 ms for $N = 10^6$ were necessary. We calculated the distance between the target and reference peaks on each histogram using the autocorrelation method suggested in [3]. The best result was calculated as the mean of the 20 different measurements. In all the measurements taken, only the scattered signal was attenuated, whereas the reference peak was kept constant, this being regarded as representative of a measurement situation when only the distance of the target changes, since the scattered signal is the only one affected by attenuation of the detected signal. The standard deviation of the distance for the 20 independent measurements can be regarded as a good estimate of the depth resolution of the system for any value of N. The resulting plot of depth resolution versus the total integrated number of photon events N is shown in figure 4.

Just like in the case of the experimental results, 20 simulated data sets were created for each of $N = 10, 3 \times 10$, $10^2, 3 \times 10^2, 10^3, 3 \times 10^3, 10^4, 3 \times 10^4, 10^5$ and 3×10^5 and the same autocorrelation analysis was applied. The standard deviation of the distance for each of the seven different values of integrated photon return is plotted alongside the experimental results in figure 4. It can be seen from the logarithmic plot of figure 4 that there is good agreement between the experimental and simulated data across almost five orders of magnitude in integrated return photons.

Assuming Poissonian statistics for the data in the measurements, the uncertainty in the distance calculated as above is the standard deviation, which is given by the formula

$$\bar{\sigma} = \frac{\sigma}{\sqrt{N}} \quad (2)$$

where σ is the mean timing jitter of the whole system in each measurement. Equation (2) implies that the gradient of figure 4, which is logarithmic in terms of both axes, should be -2.

The total resolution of the system depends both on the reference and on the target peak resolution. It is given by the following formula:

$$\sigma_{tot} = (\sigma^2_{reference} + \sigma^2_{target})^{1/2}. \quad (3)$$

Since the reference peak is kept to its maximum, it always has the same resolution, whereas the term given by the target increases. For $N < 10^5$ the term due to the reference becomes negligible, so the experimental data in figure 4 follow a straight line except for $N > 10^5$ and for $N < 100$, for which the noise becomes quite important. By applying the least squares method we deduced the straight line that best fits the data. If m is the gradient of the straight line, then the best fitting of the data shown in figure 4 corresponds to

$$m = -2.09 \pm 0.14$$

for the simulated data and

$$m = -2.01 \pm 0.21$$

for the experimental data, which shows that good agreement with the predicted result is obtained in both cases.

In figure 4 the experimental data show a resolution which is always worse than the simulated one. This arises from the fact that the simulated histograms have no background noise, whereas the experimental ones have a very small amount of noise which is caused by 'dark' events and/or temporally uncorrelated photon events (which are typically caused by ambient light levels). We therefore studied the depth resolution, taking into account different background levels.

We define the signal-to-background ratio (SBR) as the ratio between the maximum peak height and the background level and take into account the influence that it has on the signal-to-noise ratio obtained in the actual measurements (SNR). Let us denote by n_{PK} and n_B the recorded counts per channel corresponding to the peak photon intensity and to the background respectively; by $(SNR)_P$ or η_P the SNR value limited only by the photon statistics (that is, the value would be obtained without any background) and by η the actual SNR in the measurement:

$$(SNR)_P = \eta_P = \sqrt{n_{PK}} \quad (4)$$

$$SBR = \beta = \frac{n_{PK}}{n_B} \quad (5)$$

$$SNR = \eta = \frac{n_{PK}}{(n_{PK} + n_B)^{1/2}} = \eta_P \left(\frac{\beta}{\beta + 1}\right)^{1/2}. \quad (6)$$

Equation (6) shows that the value of the actual SNR is close to the ideal one $(SNR)_P$ only as long as the SBR is very high ($\beta \gg 1$). When the SBR becomes lower, a significant reduction of the SNR is met as soon as the SBR approaches a value of 5 and the SNR then rapidly falls as the SBR is further reduced. Under such conditions, the mean timing jitter is expected to be correspondingly and progressively degraded.

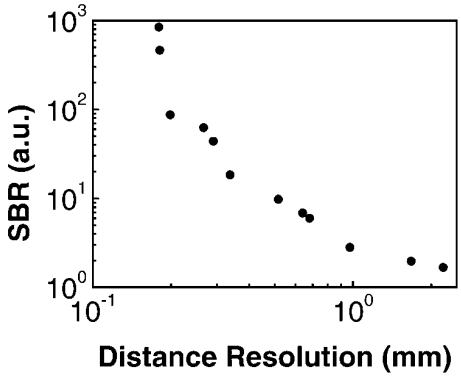

Figure 5. The signal-to-noise ratio versus the distance resolution for $N = 1000$. The graph shows the distance resolution for twelve different background values, with 20 data sets simulated for each of these data points.

In order to gain quantitative insight in this effect, 20 simulated data sets were constructed for $N = 1000$ for several different SBR by utilizing the model described in equation (2). Figure 5 shows the depth resolution (or more specifically the standard deviation from the mean depth) plotted against the SBR. As expected, the resolution gets significantly worse as the SBR decreases and has a minimum non-zero value for high values of SBR, as described in equation (2). The results shown in figure 5 indicate that the depth resolution is degraded by an increase in the background level. For example, in a very long distance measurement the scattered signal will be less intense, because of the $1/r^2$ effect of the distance, r, between the target and the detector on the photon return. Therefore the distance resolution could be significantly worse than that calculated above according to equation (3). The results in figure 4 can be regarded as a lower limit, under good measuring conditions. Further studies on the important effects of the background level will be carried out in future. One point to note about long distance ranging is the effect of 'aliasing', whereby confusion between pulses can arise when the round-trip time is greater than the period between pulses. In the measurements presented in this paper there was no confusion about which pulse had been measured because of our choice of a known fibre length which determines the delay between reference and target returns.

4. Conclusions

In this paper, we have presented experimental and simulated results showing the depth resolution obtained over five orders of magnitude in integrated photon return, N, from the target. According to the results of our study, a resolution of 3 mm can be achieved with only ten photons scattered from the target, when an overall instrumental FWHM response of $\simeq$34 ps is used.

Whilst these results presented are impressive, they serve only as an upper limit of the possible depth resolution of this technique for any given value of N, since the effect of increasing background level will degrade the depth resolution obtainable with this system. The maximum SBR, defined as the ratio of the peak height to the background, is essential for optimum exploitation of this technique. Therefore, great

care must be taken to use detectors with minimal dark count rates and that ambient light (or other temporally uncorrelated light signals) is suppressed by effective use of spatial and spectral filtering. The uses for the techniques described in this paper could be in millimetre ranging of long distances in, for example, defence and architectural applications, or in micrometre-resolution ranging of precision engineering components over relatively short ranges (up to 50 m).

Acknowledgments

This study forms part of a collaboration between the Departments of Physics and Computing and Electrical Engineering of Heriot-Watt University, British Aerospace–Sowerby Research Centre and Edinburgh Instruments, Ltd and has been supported financially by the UK Engineering and Physical Sciences Research Council through their Integrated Machine Vision Initiative. We thank Professor Efim Portnoi, Ioffe Institute, St Petersburg for the supply of the picosecond Q-switched diode lasers. We acknowledge useful discussions with Dr Manickam Umasuthan and Professor John Rarity.

References

[1] Massa J S, Buller G S, Walker A C, Cova S, Umasuthan M and Wallace A M 1998 Time-of-flight optical ranging system based on time-correlated single-photon counting *Appl. Opt.* **37** 7298–304

[2] Massa J S, Wallace A M, Buller G S, Fancey S J and Walker A C 1997 Laser depth measurement based on time-correlated single-photon counting *Opt. Lett.* **22** 543–5

[3] Umasuthan M, Wallace A M, Massa J S, Buller G S and Walker A C 1998 Processing time-correlated single photon counting data to acquire range images *Proc. IEE* **145** 237–43

[4] Alferov Z I, Zuravlev A B, Portnoi E L and Stel'makh N M 1986 Picosecond pulses from Q-switched heterostructure injection lasers *Sov. Tech. Phys. Lett.* **12** 452–3

[5] Cova S, Ghioni M, Lacaita A, Samori C and Zappa F 1996 Avalanche photodiodes and quenching-circuits for single-photon detection *Appl. Opt.* **35** 1954–76

[6] Lacaita A, Ghioni M and Cova S 1989 Double epitaxy improves single-photon avalanche diode performance *Electron. Lett.* **25** 841–3

[7] Cova S, Lacaita A, Ghioni M and Ripamonti G 1989 20-ps timing resolution with single-photon avalanche diode *Rev. Sci. Instrum.* **60** 1104–10

[8] Becker & Hickle 1995 *SPC-300 Time-Correlated Single Photon Counting. Operating Manual*